Dual-band-notched UWB MIMO antennas with miniaturization using half-cutting technology

Zhonghong Du, Xiaohui Zhang, Peiyu Qin, Yanning Yuan, Jiangfan Liu and Xiaoli Xi [ID]

The Faculty of Automation and Information Engineering, Xi'an University of Technology, Xi'an 710048, China

CAMBRIDGE
UNIVERSITY PRESS

Abstract

A compact four-element ultra-wideband (UWB) multiple-input–multiple-output (MIMO) antenna with dual polarization and dual-notched capabilities was developed and fabricated. The MIMO antenna is composed of four orthogonally placed half-cutting UWB antenna elements. This orthogonal placement improves the isolation. Furthermore, an L-shaped slot and a continuous bending slot are etched to realize the band-rejection function in the WiMAX and WLAN bands. The result shows that the antenna achieved operating bands of 2.9–16.5 GHz (140.2%, $S_{11} < -10$ dB), fully covering the UWB (3.1–10.6 GHz). The port isolation is greater than 23 dB in the frequency band of interest, excluding two rejected bands. Moreover, the MIMO antenna has excellent diversity performance, such as a low envelope correlation coefficient (<0.004), high diversity gain (approximately 10 dB), and good omni-directional radiation characteristics.

Introduction

Ultra-wideband (UWB) technology has important applications and good prospects in the broadband ultra-high-speed data transmission and short-distance communication. Nevertheless, UWB systems are susceptible to interference from multipath fading and existing narrow frequency bands, thus affecting the signal transmission quality. Usually, it is a cogent method to reduce the impact of multipath fading by using multiple-input–multiple-output (MIMO) antenna technology. It improves the channel capacity and link quality without increasing the signal power [1]. Furthermore, the overall size of the MIMO antenna swells as the number of elements increases. Thus, there are three basic requirements when designing UWB MIMO antennas: high isolation, compact size, and multiple notches.

In recent years, to address these issues, many researchers have studied the miniaturization technology [2–6], decoupling technology [7–20], and notch technology [1, 16, 19] of UWB MIMO antennas. The miniaturization technology mainly includes half-cutting technology [3, 4], bending technology [5], and fractal technology [6]. The decoupling technology comprises a defective ground structure [7, 8], reasonable layout of antenna elements (orthogonal placement [9–12] and inverted placement [7]), floor decoupling stubs [13, 14, 16], neutralization line technology [17], electromagnetic metamaterials [18], etc. Similarly, the notch technology contains etching slots [1, 16], loading electromagnetic band-gap structure [4], embedding parasitic resonance structure [19, 20], and so on.

In a previous study [3], the symmetrical half-cut technique was used to reduce the size of the antenna by 49%. Similarly, Ghahremani *et al.* [4] employed symmetrical half-cutting technology and appropriately adjusted the position of the antenna feed to achieve a 60% reduction in the size of the antenna. In another report [7], an MIMO antenna with a size of 50×35 mm^2 was proposed. It achieved more than 25 dB of isolation by etching the defective ground structure. A four-element MIMO antenna with a size of 58×58 mm^2 was reported. Furthermore, in an earlier study [15], high isolation ($S_{21} > 18$ dB) was obtained by four orthogonally placed radiators, and a hexagonally shaped complementary split-ring resonator was etched for the dual-band rejection function. In another research study [18], two novel metamaterial split-ring resonators were utilized to reduce mutual coupling, which expanded the impedance bandwidth of MIMO antennas at the same time.

A dual-band-notched four-element UWB MIMO antenna based on polarization diversity is presented in this paper. First, the miniaturization of a single UWB antenna is realized using the half-cutting technique. Second, without adding any decoupling structure, the isolation of the MIMO antenna is more than 23 dB in the UWB (excluding the notch band) through the orthogonal polarization diversity technique. Finally, the notch characteristics of the 3.1–3.9 and 5.2–5.9 GHz bands are realized by introducing L-shaped and continuous bending slots of different lengths in the radiation patch. Computer simulation technology (CST) Microwave Studio software was used to perform the simulation and analysis of the MIMO antenna.
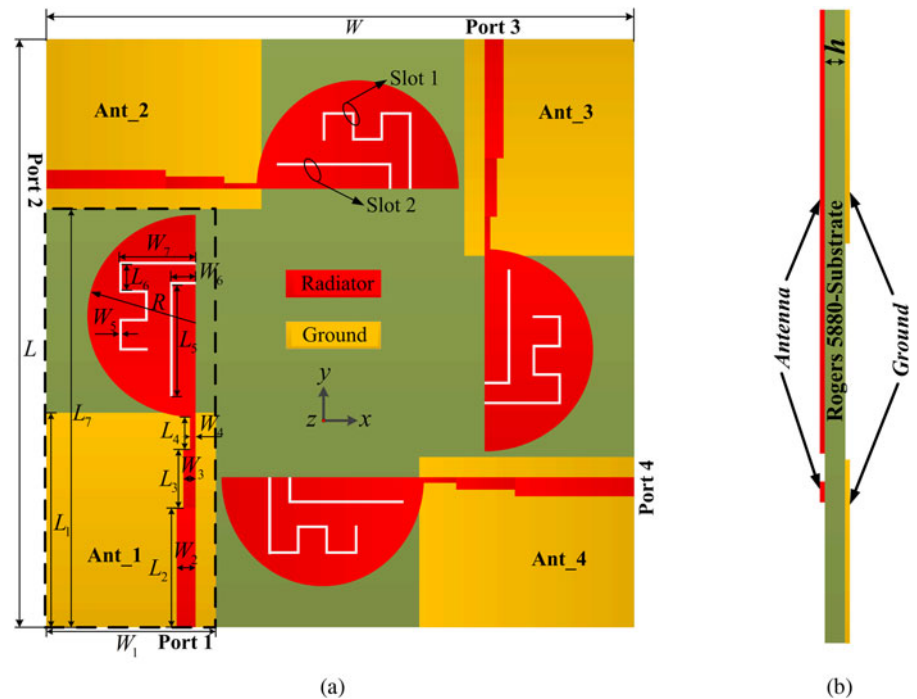
Fig. 1. Proposed design structure: (a) antenna structure and (b) side view.

Design process and simulation results

Figure 1 displays the final structure of the dual-band-notched four-element UWB MIMO antenna. A single UWB antenna is obtained by symmetrically cutting the traditional circular mono-pole UWB antenna, as shown in Fig. 2(a). The feed mode of the antenna is a three-segment transmission, and the impedance matching network can be better matched with 50 Ω by adjusting the size of each transmission line. The four antenna elements are placed on the same dielectric substrate in an orthogonal manner to realize the dual polarization characteristics of the MIMO antenna. Subsequently, the rejection band characteristics of WiMAX and WLAN bands are realized by etching slots of different lengths. The designed antenna was printed on a Rogers RT duroid/5880 substrate with a relative permittivity of 2.2, loss tangent of 0.0009, and thickness $h = 0.508$ mm.

UWB antenna element design

In general, if only the change in the effective length of the antenna is considered, the antenna is half-cut at the axis of symmetry,

which does not affect its performance. The principle is attributed to the magnetic wall effect at the symmetry plane of the antenna with a symmetric structure; thus, the halved antenna still has the frequency characteristics required by the resonance frequency. Figure 2(a) shows the design process of a single UWB antenna. A miniaturized antenna (#2) can be obtained by halving the original antenna (#1) along the axis of symmetry (SS'). As shown in Fig. 2(b), the reflection coefficient of the halved antenna is significantly worse than that of the original antenna because the input impedance of the halved antenna changes and its resonance frequency is basically unchanged. To improve the impedance matching of the halved antenna, the position of the antenna (#3) on the dielectric substrate is appropriately adjusted. Figure 2(b) shows that #3 has reflection characteristics similar to those of #1, and #3 has a wider operating band.

Band-notch structure design

A 90° clockwise rotation is utilized to create a four-port MIMO array after the basic UWB antenna unit (#3) is designed. Adjacent antenna units are then distributed orthogonally to
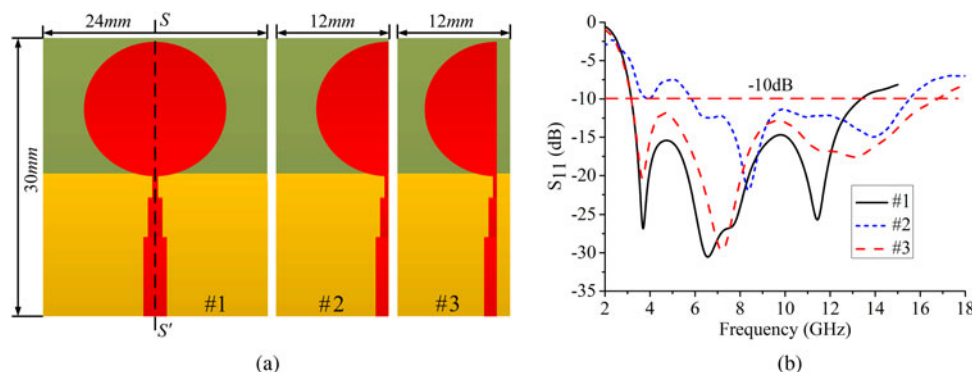

Fig. 2. Evolution of the single UWB antenna: (a) original antenna structure and (b) S_{11}.
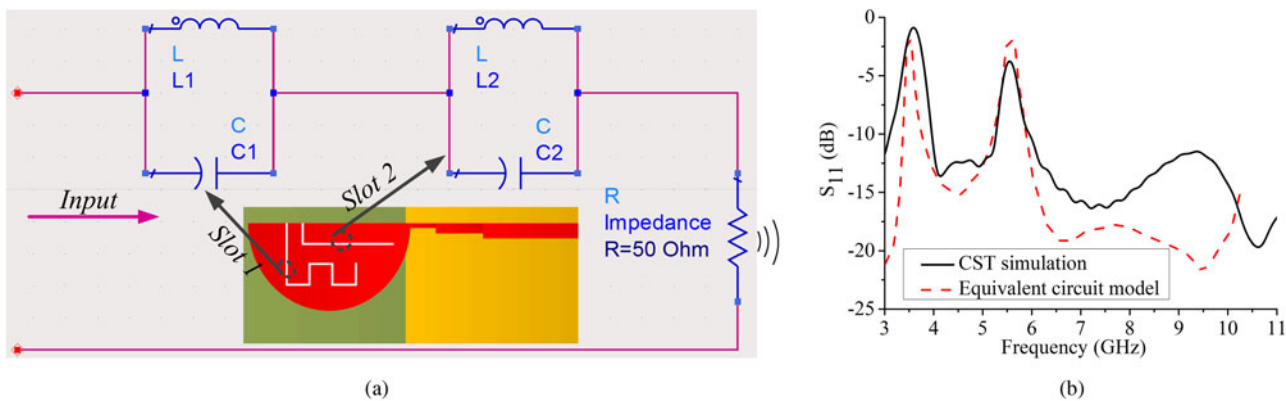
Fig. 3. Comparison between the simulated S_{11} of antenna by CST and by the equivalent circuit model: (a) equivalent circuit model and (b) S_{11}.

each other, and the polarization characteristics correspond to orthogonal polarization. In this way, the antenna units can only receive weak signals excited by each other; thus, the isolation of the MIMO antenna is improved. The proposed MIMO antenna structure also exhibits an L-shaped and continuous bending-type slot structure on the radiator, and the direction of the current is opposite in these two slots. The radiated fields caused by the adverse current can cancel each other out, so the antenna cannot radiate efficiently in the notched frequency bands [13].

The length of the two slot structures is related to the center frequency of the notch band, and it can be calculated approximately according to equation (1) [20]:

$$L = \frac{\lambda}{4} = \frac{c}{4f_0\sqrt{\varepsilon_{eff}}}, \; \varepsilon_{eff} = \frac{\varepsilon_r + 1}{2} \quad (1)$$

In equation (1), L is the slot length, c is the speed of light, and ε_{eff} and ε_r are the effective permittivity and relative permittivity, respectively.

According to equation (1), the length of the slot is optimized to be approximately equal to the length of $\lambda/4$ (where λ is the free-space wavelength in the notch center frequency). When the antenna operates in the notch frequency band, these slots can be regarded as the $\lambda/4$ transmission line with a terminal short circuit at the corresponding frequency, i.e. the parallel resonant circuit. The equivalent circuit of the antenna is shown in Fig. 3(a). Whenever any slot resonates, the input impedance of the antenna at the corresponding notch band approaches infinity. At this time, the resonant circuit is equivalent to an open circuit, and the antenna cannot transmit energy normally; thus, a notch band is generated. In Table 1, the calculation and simulation slot length values when the notch center frequencies are 3.5 and 5.5 GHz, respectively, are compared. Table 1 shows that the difference between the two values is very small.

Figure 3(b) shows a comparison between S_{11} of the proposed antenna obtained by CST simulation and the equivalent circuit model. As shown in the figures, the trends of the curves agree reasonably well over the UWB band, especially in the dual-notched frequency bands. The discrepancy between the curves can be mostly attributed to the antenna that is replaced by a 50 Ω resistance in the equivalent circuit. In most cases, if the antenna is well matched, this approximation can be valid, but for a large bandwidth this hypothesis is not fulfilled.

Table 1. Comparison of theoretical value and simulation value of slot length

	Frequency (GHz)	Theoretical calculation (mm)	Full-wave simulation (mm)
Slot 1	3.5	16.9	17.4
Slot 2	5.5	10.7	11.0

All the parameters of the proposed antenna were optimized using commercial full-wave software CST Microwave Studio. The final detailed dimensions of the UWB MIMO antenna, in millimeters, are as follows: $W = 42$, $W_1 = 12$, $W_2 = 1.5$, $W_3 = 1.2$, $W_4 = 0.4$, $W_5 = 0.2$, $W_6 = 2$, $W_7 = 6$, $L = 42$, $L_1 = 14.65$, $L_2 = 8$, $L_3 = 4.3$, $L_4 = 2$, $L_5 = 8.8$, $L_6 = 2$, $L_7 = 30$, $R = 7.7$, $h = 0.508$.

Simulated and experimental results and analysis

The fabricated antenna prototype and the test environment are shown in Fig. 4. The 3671E vector network analyzer (China Electronics Technology Instruments Limited Company) was used to test parameters, such as S-parameters and isolation.

S_{11}-parameters

The simulated and measured S_{11} of the antenna prototype is given in Fig. 5(a), showing similar trends. The measured −10 dB impedance bandwidth is 2.9–16.5 GHz (relative bandwidth is about 140.2%), which is close to the simulated result (2.7–16.7 GHz, relative bandwidth is about 144.3%). The notch frequency bands of the MIMO antenna are 3.1–3.8 and 5.2–5.9 GHz. In addition, Fig. 5(a) also depicts the S_{11} of the slotless MIMO antenna, and the results are acceptable.

Figure 5(b) shows the simulated surface current distribution of the antenna at 3.5 and 5.5 GHz. Near the center frequency of the notch, a large number of currents in the opposite directions are confined along the slot structure, the electromagnetic energy cannot be completely radiated outward, and the notch function occurs [13, 16]. Nevertheless, the current is evenly distributed in the non-notched frequency band, and the antenna energy is normally radiated outward.

To analyze the effect of slits on the band-notched characteristics, various parameters were assessed. First, the length of the notch antenna, slot 1, is varied to show the effect of the overall length of slot 1 on the WiMAX band-notched frequency in
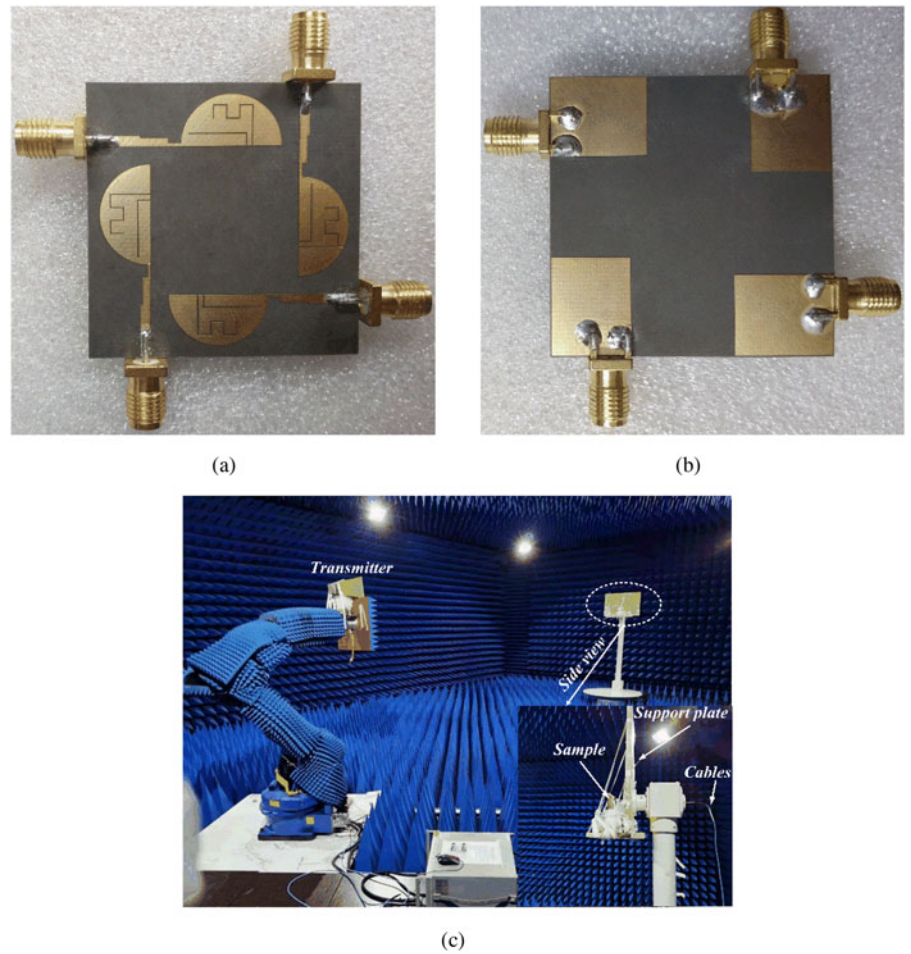
Fig. 4. Photograph of the fabricated antenna: (a) top view, (b) bottom view, and (c) test environment.

Fig. 6(a). As the figure shows, when the length of slot 1 is shifted from 16.8 to 18 mm, the notch band shifts toward a lower frequency. Therefore, to obtain the desired band-notched frequency, 17.4 mm is chosen as the final value. Similarly, Fig. 6(b) shows the *S*-parameters for the variation of length slot 2, while other parameters remain constant. As the length of slot 2 increases from 10.5 to 11.5 mm, the center of the notched frequency band shifts from 5.9 to 5.3 GHz. Therefore, 11 mm is chosen as the final value of the slot 2 length. Both values are approximately the same, which confirms the effectiveness of equation (1).

Isolation

Figure 7 shows the measured and simulated isolation of the MIMO antenna when port 1 is excited and the other three ports are terminated with 50 Ω matched loads. In the UWB frequency band, the couplings between ports 1 and 2 and that between ports 3 and 4 are less than −23 dB, but the coupling in the notch band is only less than −20 dB. This is because there is substantial energy accumulation in the notch frequency band and this energy cannot be radiated outward, which leads to the
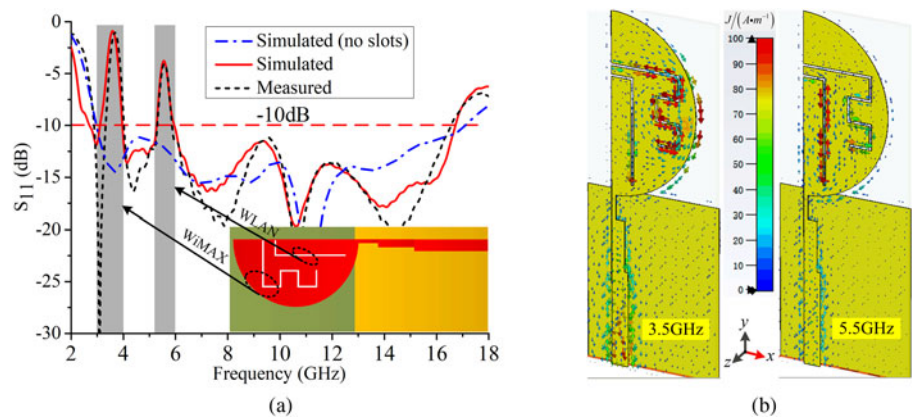

Fig. 5. S_{11} and simulated surface current distribution of MIMO antenna: (a) S_{11} and (b) surface current distribution.
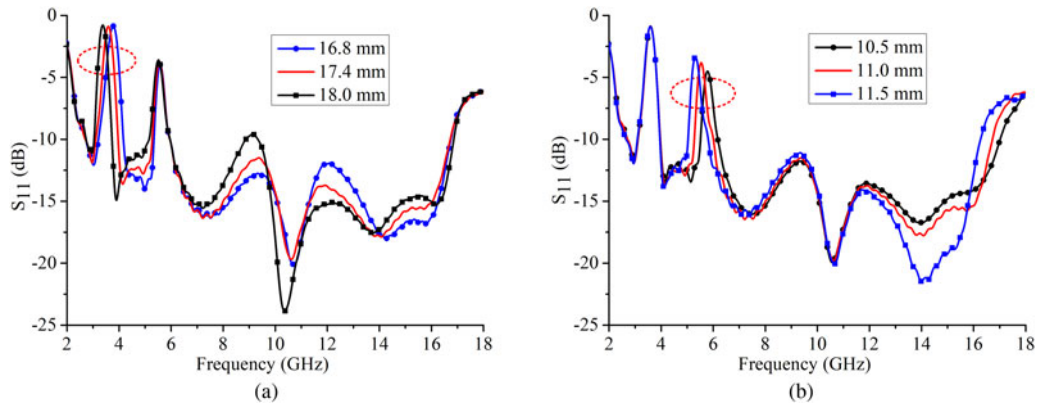
Fig. 6. Effects of the length variation of the slits on S_{11}: (a) slot 1 and (b) slot 2.
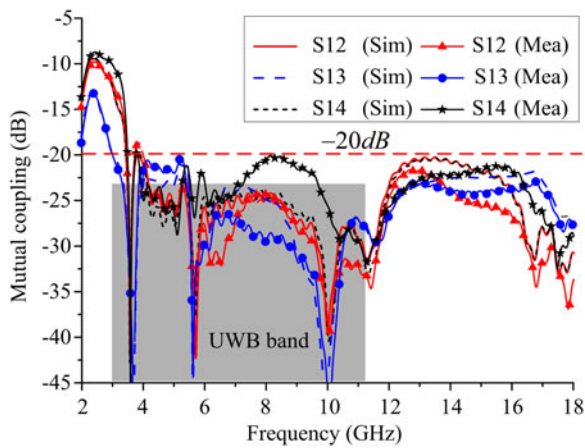

Fig. 7. Isolation of the UWB MIMO antenna.

increase of the coupling between antenna elements. Because of the symmetrical geometry of the structure, the same characteristics appear when the other three ports are activated.

To understand the decoupling effect of the polarization diversity technology intuitively, Fig. 8 shows the simulated surface current distribution of the MIMO antenna at 10 GHz. When port 1 is excited, the surface current flows along the y-axis direction and forms a y-polarized field. Therefore, the surface current coupled to the other three antenna elements is very weak. Similarly, when port 2 is excited, the surface current flows in the x-direction, forming an x-polarized field. A large amount of current is concentrated in this antenna element, while the other three antenna elements have weak surface currents. The polarization diversity technology can effectively improve the isolation of MIMO antennas.

Radiation characteristics

In a MIMO system, multiple antenna elements with different radiation patterns can be employed to reduce the multipath effects. Figure 9(a) shows the three-dimensional (3D) radiation pattern of the MIMO antenna when ports 1–4 are excited at 5 GHz. As shown in the figure, the radiation patterns of Ant_1 and Ant_3 are 180° mirror images, and the radiation patterns of Ant_1 and Ant_2 are perpendicular to each other. Furthermore, Ant_2 has a good omnidirectional radiation mode in the yoz-plane, and a radiation pattern similar to the "8"-shape in the xoz-plane. In addition, the two-dimensional (2D) radiation patterns of Ant_1 and Ant_2 in the xoy-plane at 5 GHz are plotted in Fig. 9(b). The results show that the radiation patterns of ports 1 and 2 in the xoy-plane are also perpendicular
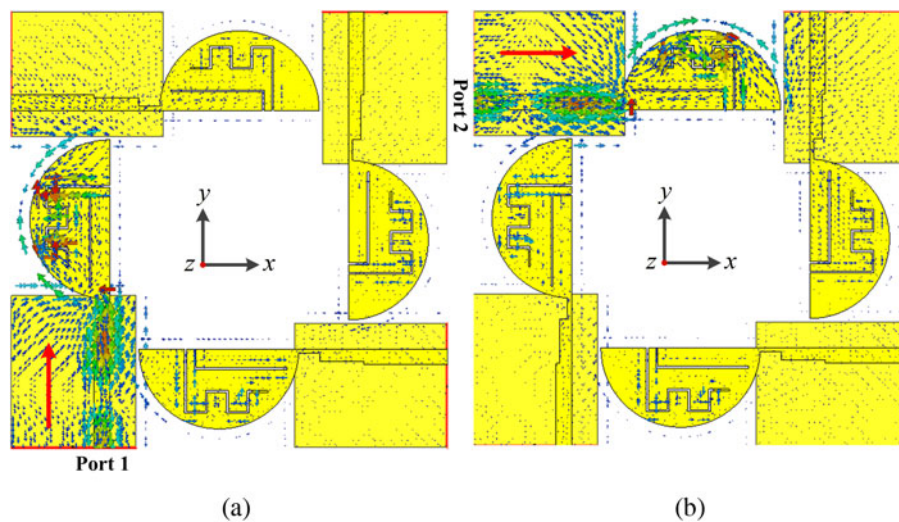

(a)   (b)

Fig. 8. Simulated surface current distribution on the antenna at 10 GHz: (a) port 1 is excited and other ports are matched and (b) port 2 is excited and other ports are matched.
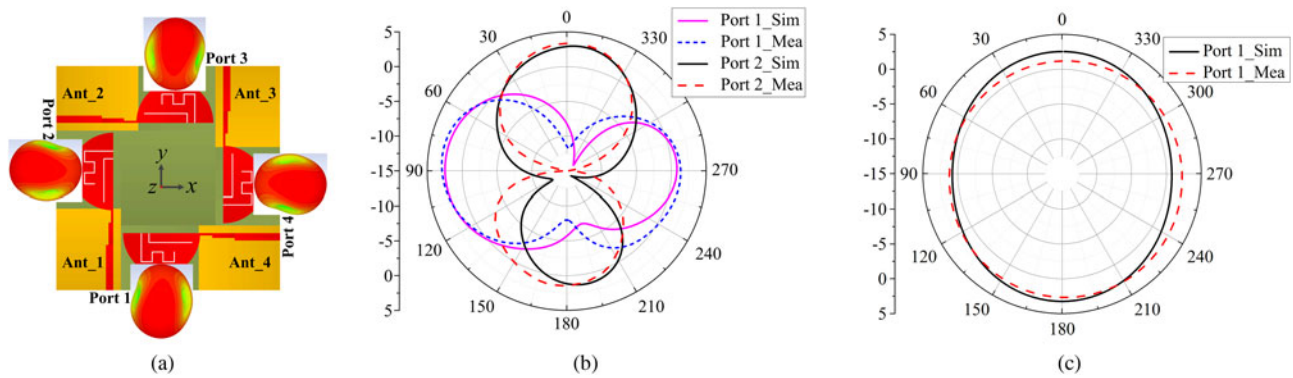
Fig. 9. 3D and 2D patterns of the antenna when exciting different ports: (a) 3D pattern, (b) *xoy*-plane, and (c) *xoz*-plane (only port 1 is excited, while the other ports are terminated with a 50 Ω load).
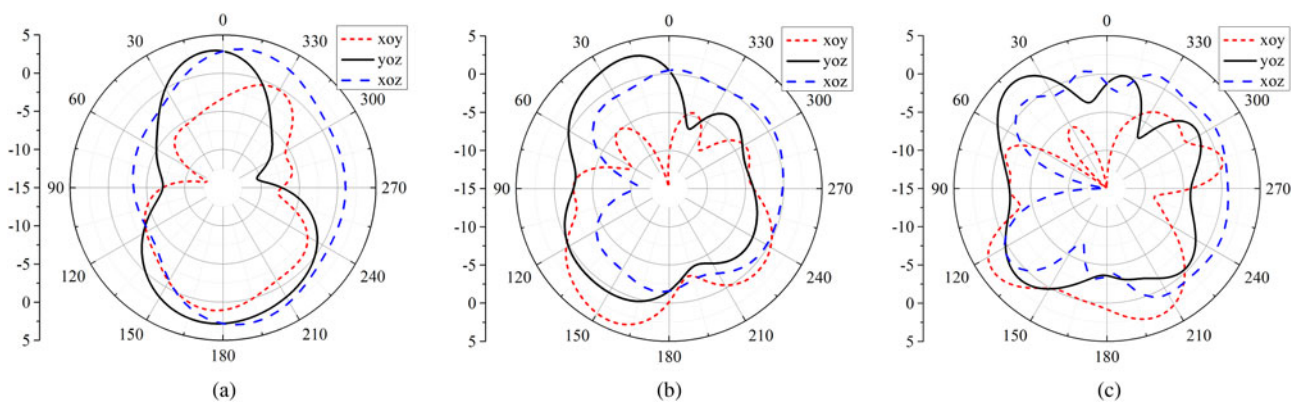

Fig. 10. Simulated radiation patterns of the MIMO antenna: (a) 8 GHz, (b) 11 GHz, and (c) 14 GHz.
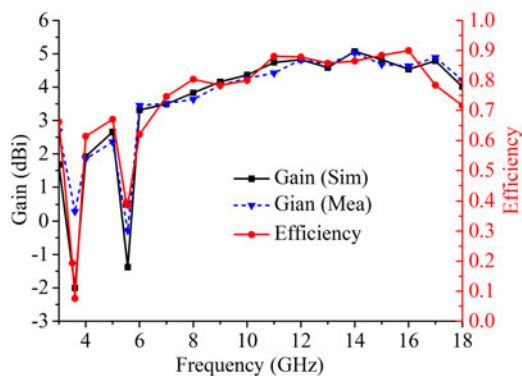

Fig. 11. Gain and efficiency of the UWB MIMO antenna.
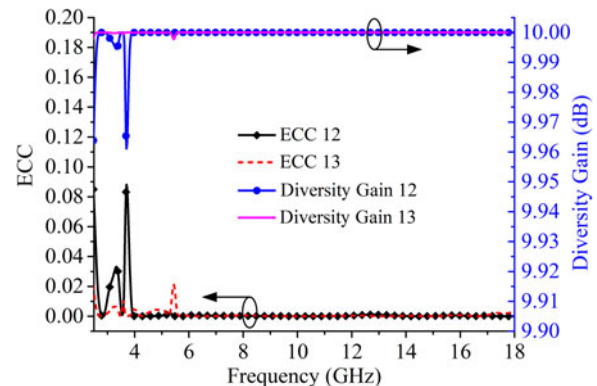

Fig. 12. Simulated ECC and DG of the proposed design.

to each other. Furthermore, Ant_1 has stronger radiation at 90° and 270°, whereas Ant_2 has null radiation in those directions. The above results verify that the proposed MIMO antenna has good diversity performance. Figure 9(c) shows that the pattern is nearly omnidirectional in the *xoz*-plane, which is suitable for UWB MIMO systems.

To illustrate the radiation stability of the proposed antenna, Fig. 10 shows the simulated radiation patterns of the antenna at 8, 11, and 14 GHz when port 1 is excited, while the other port is terminated with a 50 Ω load, and *vice versa*. At lower frequencies, the patterns were fairly "8"-shaped in the *xoy*-plane and

omnidirectional in the *xoz*-plane, as shown in Figs 9(b) and 10(a) at 5 and 8 GHz. At higher frequencies, radiation patterns deteriorate at higher frequencies owing to the splitting of the radiation lobes. The deterioration is caused by an imbalance in the high-frequency current distribution [7].

Figure 11 shows that, in the operating band, the maximum gain of the antenna is approximately 5 dBi. In the notch band, the gain plummets to −2 dBi, which effectively solves the problem of electromagnetic compatibility among the UWB, WiMAX, and WLAN. The radiation efficiency of the antenna also has the same variation trend.

Table 2. Performance comparisons with previously reported antennas

Ref.	No. of elements	Antenna size (mm²)	Bandwidth (GHz)	Maximum gain (dBi)	Isolation (dB)	ECC
[6]	4	45 × 45	2.0–10.6	4.8	>17	<0.005
[9]	2	25 × 50	2.4–17.1	5.4	>25	<0.001
[10]	4	40 × 40	2.4–10.6	–	>20	<0.02
[11]	4	45 × 45	2.0–16.8	4.0	>22	<0.01
[12]	4	41 × 41	2.96–11.4	4.0	>20	<0.03
[20]	4	50 × 50	2.0–12.0	5.9	>17	<0.15
This study (#3$_{MIMO}$)	4	42 × 42	2.7–16.5	5.0	>23	<0.004
#1$_{MIMO}$	4	54 × 54	3.25–16.5	6.2	>15	<0.01

MIMO performance parameters

In a MIMO antenna system, the envelope correlation coefficient (ECC) is used to evaluate the diversity performance. In an ideal uniform scattering environment, S-parameters – equation (2) – are often used to calculate the ECC [6, 9]. However, the calculated ECC is closer to the actual situation with the far-field parameters – equation (3) [7]:

$$ECC = \rho_{eij} = \left| \frac{|S_{ii}^* S_{ij} + S_{ji}^* S_{jj}|}{|(1 - |S_{ii}|^2 - |S_{ij}|^2) \cdot (1 - |S_{ji}|^2 - |S_{jj}|^2)|^{1/2}} \right|^2 \quad (2)$$

reports have been shown in Table 2. Compared with those reported earlier [6, 11, 12], the proposed antenna has a higher gain. Moreover, Table 2 shows the related parameters of the MIMO antennas (#1$_{MIMO}$ and #3$_{MIMO}$) designed with a full antenna (#1) and a halved antenna (#3) as a single antenna. In the comparison, #3$_{MIMO}$ has great advantages in terms of size and isolation.

Conclusion

A compact (42 × 42 mm²) dual-band-notched four-element UWB MIMO antenna was proposed. A single UWB antenna was miniaturized using half-cut technology. On the one hand,

$$\rho_{eij} = \frac{\left| \int_0^{2\pi} \int_0^{\pi} (XPR \cdot E_{\theta i} \cdot E_{\theta j}^* \cdot P_\theta + E_{\phi i} \cdot E_{\phi j}^* \cdot P_\phi) d\Omega \right|^2}{\int_0^{2\pi} \int_0^{\pi} (XPR \cdot E_{\theta i} \cdot E_{\theta i}^* \cdot P_\theta + E_{\phi i} \cdot E_{\phi i}^* \cdot P_\phi) d\Omega \times \int_0^{2\pi} \int_0^{\pi} (XPR \cdot E_{\theta j} \cdot E_{\theta j}^* \cdot P_\theta + E_{\phi j} \cdot E_{\phi j}^* \cdot P_\phi) d\Omega} \quad (3)$$

where i and j are the numbers of ports, XPR is the cross-polarization ratio, and P_θ and P_ϕ are the θ and ϕ components of the angular density functions of the incoming wave, respectively.

The diversity gain (DG) is also an important parameter for evaluating the performance of a MIMO antenna. The DG can be calculated using equation (4). Figure 12 shows, except for the dual-notch frequency band, the ECC is lower than 0.004, and the DG is higher than the 9.9 dB for the MIMO antenna, proving that the antenna has a good diversity characteristic:

$$DG = 10\sqrt{1 - ECC^2} \quad (4)$$

Table 2 lists the performance parameters of MIMO antennas that have been reported in the literature, and compares them with those of the proposed antenna. Compared with those in the literature [10, 12], although the antenna in this study has a larger size, it has the advantages of high isolation and a simple structure (without using any decoupling structure). In addition, compared with previously reported ones [6, 20], the design here has obvious advantages in terms of size and isolation, but the previous antennas [6, 20] have better low-frequency performance. Although a previously designed antenna [9] is smaller, it is a two-element MIMO antenna. The maximum gains in previous

the orthogonal diversity technique was used to enhance the isolation of the MIMO antenna, which can significantly improve the isolation ($S_{21} > 23$ dB) of the MIMO antenna without adding other decoupling structures. On the other hand, two slots with different lengths were etched on the radiator to realize the band rejection characteristics of the WiMAX and WLAN frequency bands. In addition, the advantages of orthogonal placement were analyzed using the 2D and 3D radiation patterns.

References

1. **Gómez-Villanueva R and Jardón-Aguilar H** (2019) Compact UWB uniplanar four-port MIMO antenna array with rejecting band. *IEEE Antennas and Wireless Propagation Letters* **18**, 2543–2547.
2. **Das S, Chowdhury P and Biswas A** (2015) Analysis of a miniaturized multiresonant wideband slotted microstrip antenna with modified ground plane. *IEEE Antennas and Wireless Propagation Letters* **14**, 60–63.
3. **Liu J, Esselle KP and Hay SG** (2014) Effects of printed UWB antenna miniaturization on pulse fidelity and pattern stability. *IEEE Transactions on Antennas and Propagation* **62**, 3903–3910.

4. **Ghahremani M, Ghobadi C and Nourinia J** (2019) Miniaturised UWB antenna with dual-band rejection of WLAN/WiMAX using slitted EBG structure. *IET Microwaves, Antennas and Propagation* **13**, 360–366.
5. **Sun J, Fang H, Lin P and Chuang C** (2016) Triple-band MIMO antenna for mobile wireless applications. *IEEE Antennas and Wireless Propagation Letters* **15**, 500–503.
6. **Tripathi S, Mohan A and Yadav S** (2015) A compact Koch fractal UWB MIMO antenna with WLAN band-rejection. *IEEE Antennas and Wireless Propagation Letters* **14**, 1565–1568.
7. **Wang L, Du Z and Yang H** (2019) Compact UWB MIMO antenna with high isolation using fence-type decoupling structure. *IEEE Antennas and Wireless Propagation Letters* **18**, 1641–1645.
8. **Chattha HT, Latif F and Tahir FA** (2019) Small-sized UWB MIMO antenna with band rejection capability. *IEEE Access* **7**, 121816–121824.
9. **Dastranj A** (2017) Low-profile ultra-wideband polarisation diversity antenna with high isolation. *IET Microwaves, Antennas and Propagation* **11**, 1363–1368.
10. **Rajkumar S, Amala AA and Selvan KT** (2019) Isolation improvement of UWB MIMO antenna utilising molecule fractal structure. *Electronics Letters* **10**, 576–579.
11. **Pannu P and Sharma DK** (2020) A low-profile quad-port UWB MIMO antenna using defected ground structure with dual notch-band behavior. *International Journal of RF and Microwave Computer-Aided Engineering* **30**, 1–13.
12. **Mchbal A, Touhami NA and Elftouh H** (2020) Coupling reduction using a novel circular ripple-shaped decoupling mechanism in a four-element UWB MIMO antenna design. *Journal of Electromagnetic Waves and Applications* **4**, 1–20.
13. **Chandel R, Gautam AK and Rambabu K** (2018) Tapered fed compact UWB MIMO-diversity antenna with dual band-notched characteristics. *IEEE Transactions on Antennas and Propagation* **66**, 1677–1684.
14. **Thakur E, Jaglan N and Gupta SD** (2020) Design of compact triple band-notched UWB MIMO antenna with TVC-EBG structure. *Journal of Electromagnetic Waves and Applications* **11**, 1601–1615.
15. **Kumar P, Urooj S and Alrowais F** (2020) Design and implementation of quad-port MIMO antenna with dual-band elimination characteristics for ultra-wideband applications. *Applied Sciences* **5**, 1–12.
16. **Gautam AK, Yadav S and Rambabu K** (2018) Design of ultra-compact UWB antenna with band-notched characteristics for MIMO applications. *IET Microwaves, Antennas and Propagation* **12**, 1895–1900.
17. **Zhang S and Pedersen GF** (2016) Mutual coupling reduction for UWB MIMO antennas with a wideband neutralization line. *IEEE Antennas and Wireless Propagation Letters* **15**, 166–169.
18. **Wang C, Yang XS and Wang BZ** (2020) A metamaterial-based compact broadband planar monopole MIMO antenna with high isolation. *Microwave and Optical Technology Letters* **5**, 1–6.
19. **Chandel R and Gautam AK** (2016) Compact MIMO/diversity slot antenna for UWB applications with band-notched characteristic. *Electronics Letters* **52**, 336–338.
20. **Khan MS, Iftikhar A and Shubair R** (2020) A four element, planar, compact UWB MIMO antenna with WLAN band rejection capabilities. *Microwave and Optical Technology Letters* **62**, 1–8.

Zhonghong Du received his B.S. in Electronic Information from Hexi University, Zhangye, China in 2017 and his M.S. in Communicating Engineering from the Xi'an University of Technology, Xi'an, China in 2020. He is currently pursuing his Ph.D. degree with the Department of Electronic Engineering, Xi'an University of Technology. His research interests include MIMO antennas decoupling technology, electromagnetic metasurface, and RF circuits.

Xiaohui Zhang received his B.S. in Industrial Automation in 1995, his M.S. in Control Science and Engineering in 2002, and his Ph.D. degree in Control Science and Engineering in 2009, all from the Xi'an University of Technology, Xi'an, China. He is currently a Professor of Information and Control Department at the Xi'an University of Technology, Xi'an, China. His recent research interests include advanced navigation, signal processing and pattern recognition, electromagnetic technology, and antenna design.

Peiyu Qin received her B.S. in Information Engineering from Tianjin Normal University, Tianjin, China in 2019. She is currently a graduate student at the Xi'an University of Technology, Xi'an, China. Her current research interests include electromagnetic metasurface and MIMO antennas.

Yanning Yuan received her B.S. in Electronic Information from Liaoning Shihua University, Fushun, China in 2004 and her M.S. in Communicating Engineering from the Xi'an University of Technology, Xi'an, China in 2007. She subsequently joined the Shaanxi Lingyun Science and Technology Co., Ltd. and served as a project manager. She is currently a full-time researcher at the Xi'an University of Technology, Xi'an, China. Her research interests include ultra-wideband antennas, multi-frequency antennas, and RF circuits.

Jiangfan Liu (M'16) received his B.S. and M.S. degrees in Electronic Engineering from the Xi'an University of Technology (XUT), Xi'an, China, in 2006 and 2009, respectively, and his Ph.D. degree in Electronic Engineering from Northwestern Polytechnical University, Xi'an, in 2013. He is currently an associate professor with the Department of Electronic Engineering, XUT. His current research interests include computational electromagnetics and antenna design.

Xiaoli Xi received her B.S. in Applied Physics from the University of Defense Technology in Changsha, China in 1990, her M.S. in Biomedical Engineering from the Fourth Military Medical University in Xi'an, China in 1998, and her Ph.D. degree in Electrical Engineering from the Xi'an Jiaotong University in Xi'an, China in 2004. She is currently a Professor at the Department of Electrical Engineering at the Xi'an University of Technology, Xi'an, China. Her recent research interests include antenna design, radio wave propagation and advanced navigation, and electromagnetic technology.